

# Room-Temperature Processing of Inorganic Perovskite Films to Enable Flexible Solar Cells

*Dianyi Liu<sup>1</sup>, Chenchen Yang<sup>1</sup>, Matthew Bates<sup>1</sup>, Richard R. Lunt<sup>1,2\*</sup>*

1. Department of Chemical Engineering and Materials Science, Michigan State University,  
East Lansing, Michigan 48824, USA

2. Department of Physics and Astronomy, Michigan State University, East Lansing, Michigan  
48824, USA

\*Lead contact; E-mail: ([rlunt@msu.edu](mailto:rlunt@msu.edu))

KEYWORDS: flexible; inorganic halide perovskite; solar cells; room temperature; air processing

ABSTRACT. Inorganic lead halide perovskite materials have attracted great attention recently due to their potential for greater thermal stability compared to hybrid organic perovskites. However, the high processing temperature to convert from the non-perovskite phase to cubic perovskite phase in many of these systems has limited their application in flexible optoelectronic

devices. Here, we report a room temperature processed inorganic PSC based on CsPbI<sub>2</sub>Br as the light harvesting layer. By combining this composition with key precursor solvents, we show that the inorganic perovskite film can be prepared by the vacuum-assist method under room temperature conditions in air. Unencapsulated devices achieved the power conversion efficiency up to 8.67% when measured under 1-sun irradiation. Exploiting this room temperature process, flexible inorganic PSCs based on an inorganic metal halide perovskite material is demonstrated.

Halide perovskite materials have emerged as excellent candidates for photovoltaic applications in recent years.<sup>1-4</sup> High device efficiency and low materials costs have given perovskite solar cells (PSCs) strong potential as a competitor for silicon solar cells.<sup>5-7</sup> To date, the highest reported power conversion efficiency (*PCE*) of hybrid organic-inorganic PSCs is up to 22.7%,<sup>7,8</sup> which is higher than the efficiencies of polycrystalline silicon solar cells, cadmium telluride (CdTe) solar cells and copper-indium-gallium selenide (CIGS) solar cells. However, the stability issue of organic-inorganic halide perovskite materials is still a key challenge for the application of PSCs in commercial applications due to high volatility of organic components in hybrid perovskite compounds.<sup>9-11</sup>

In contrast, inorganic perovskite materials could have better intrinsic thermal stability.<sup>12</sup> Previous research suggests that pure CsPbI<sub>3</sub> perovskite can maintain the stable cubic phase over 400 °C.<sup>12,13</sup> Thus, significant effort has been focused on developing of PSCs with the inorganic cesium lead halide light absorbers.<sup>13-25</sup> Sutton *et al.* systematically investigated the stability behavior of the cesium lead halide compounds, and reported inorganic PSCs with a *PCE* of 9.84%.<sup>13</sup> Chen *et al.* used the vacuum-deposition method to prepare inorganic cesium halide PSCs and achieved a device efficiency over 11%.<sup>24</sup> Zeng *et al.* reported a polymer-passivated cesium lead halide PSC based on the inorganic perovskite nanocrystals with the *PCE* of over 12% and an open-circuit voltage ( $V_{OC}$ ) of over 1.3 V.<sup>17</sup> Wang *et al.* very recently reported a certified efficiency of 14.67%, which is also the highest efficiency of an inorganic perovskite solar cells to date.<sup>26</sup> Despite the rapid research progress on improving efficiencies with inorganic PSCs, the processing of inorganic perovskite film is still challenging. Because the conversion temperature of CsPbI<sub>3</sub> from the non-perovskite phase to cubic perovskite phase occurs at over 300 °C,<sup>12,13</sup> the fabrication process of CsPbI<sub>3-x</sub>Br<sub>x</sub>-based inorganic perovskite films generally

require a thermal annealing treatment at temperatures up to 350 °C.<sup>13, 15-20, 23, 24, 27</sup> The high temperature thermal annealing treatment not only increases the cost of inorganic PSCs but it can prevent the application of inorganic perovskite materials on polymer-based flexible substrates.

To reduce the operation temperature of cesium lead halide perovskite films, several approaches have been examined in the past two years.<sup>14, 28-34</sup> For example, it was shown that doping a small amount of bromide (Br) can dramatically decrease the formation temperature of CsPbI<sub>3</sub> film.<sup>35</sup> Following this work, Beal *et al.* reported the low temperature processing of CsPbBrI<sub>2</sub> film as the light absorber.<sup>14</sup> The device was fabricated under 135 °C and obtained a *PCE* of up to 6.5%. Other efforts have introduced various additives to decrease the fabrication temperature which include hydroiodic acid, bismuth iodide, sulfobetaine zwitterions, ethylammonium iodide.<sup>28-30, 32-34</sup> With these additives, the cubic phase CsPbI<sub>3-x</sub>Br<sub>x</sub> film could be formed under 90-150 °C. However, the thermal annealing treatment still remained an essential step for preparation of the cesium lead halide perovskite films.

Room temperature processing is not only important to simplify the fabrication procedure, but it also enables fabrication on flexible substrates.<sup>5</sup> To date, only two studies have reported inorganic lead halide films fabricated under room temperature that then required high temperature annealing of TiO<sub>2</sub> (450 - 500 °C) and pre-synthesized perovskite quantum dots.<sup>25, 31</sup> In addition, despite many reports of flexible solar cells based on the organic-inorganic hybrid perovskite materials, flexible inorganic perovskite solar cell have not yet been reported.<sup>5, 36-46</sup> Here, we develop a room temperature processed inorganic PSC with CsPbI<sub>2</sub>Br as the light harvesting layer. By choosing a suitable precursor solvent, combined with the vacuum assist method, we show that inorganic perovskite films can be prepared under room temperature in air with a *PCE* up to 8.67% when measured under 1-sun irradiation. We subsequently show that this

low temperature processing enables fabrication of highly flexible inorganic halide perovskite photovoltaics.

## Results and Discussion

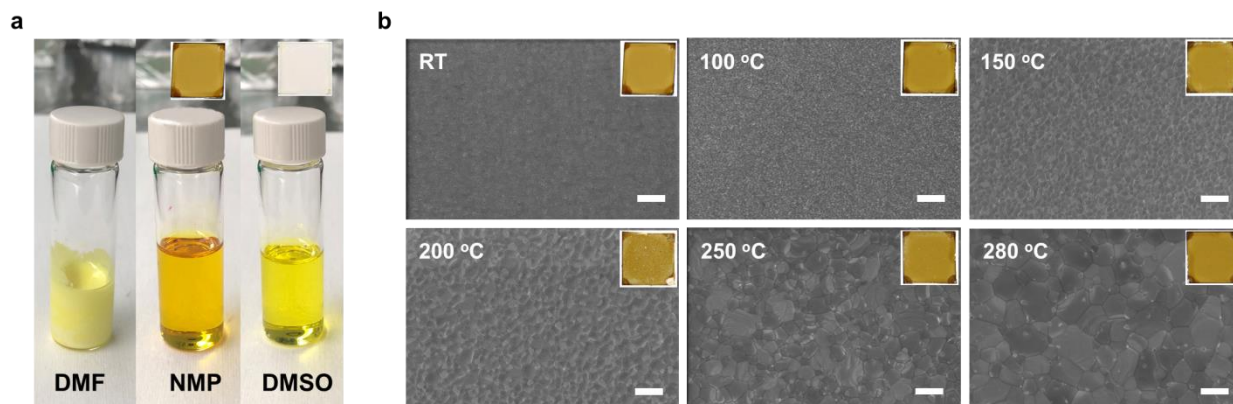


**Figure 1. Precursors Development.** (a) Photograph of CsPbI<sub>2</sub>Br precursor solutions prepared by various solvents. The inset shows the films prepared by the relative precursor solutions with the room temperature process. (b) SEM image of CsPbI<sub>2</sub>Br films with various annealing temperatures. The inset shows the photograph of the films. The scale bar is 1 μm.

Due to the limited solubility of lead halide compounds, the precursor solvents generally chosen are N,N-dimethylformamide (DMF), dimethyl sulfoxide (DMSO) and DMF/DMSO mixtures.<sup>2, 4, 47-50</sup> The solubility of mixed halide cesium lead precursors are particularly limited in DMF (Figure 1a),<sup>13</sup> leading some researchers to utilize pure DMSO.<sup>14, 16, 22, 29-30</sup> However, DMSO is a Lewis-base with strong coordination capability which can result in colorless coordination complexes with lead halide compounds,<sup>47, 51-54</sup> and lead to difficulties in converting the lead halide perovskite precursors to the perovskite phase under room temperature (Figure 1a). Another polar aprotic solvent used to fabricate organic-inorganic hybrid perovskite solar cells is 1-methyl-2-pyrrolidone (NMP).<sup>53, 55-58</sup> Compared with DMF and DMSO, NMP has good

solubility for cesium lead halide precursors and weak coordination affinity for lead compounds. NMP has other advantages as well including better crystallization of perovskite film and miscibility with other solvents, and has been reported as the solvent to fabricate hybrid organic-inorganic perovskite solar cells under room temperature.<sup>55, 57</sup> Hence, we focus on NMP as the solvent for preparation of inorganic lead halide perovskite films with room temperature processing.

It can be seen from Figure 1a that the CsPbI<sub>2</sub>Br perovskite films can be successfully prepared by the vacuum-assist deposition process under room temperature.<sup>48-49, 59</sup> After the NMP solvent was extracted from the film under vacuum, the light brown CsPbI<sub>2</sub>Br perovskite film was formed. Scanning electron microscopy (SEM) images (Figure 1b) show that the CsPbI<sub>2</sub>Br film is smooth and homogenous. Due to the rapid solvent extraction the CsPbI<sub>2</sub>Br film was formed quickly with a low level of crystallization, and lead to a grain size of ~ 50 nm. To investigate the thermal stability of the room temperature processed CsPbI<sub>2</sub>Br film, we annealed the films under various temperatures in inert atmosphere. The photograph of these films clearly shows that the films maintain a brown color from room temperature to 280 °C. The color of the 100 °C film and the 150 °C film are different from the previous report by Sutton,<sup>13</sup> but agree with the report by Beal.<sup>14</sup> We infer that the film preparation method can dramatically influence the phase conversion temperature and the thermal stability of CsPbI<sub>2</sub>Br films. Accordingly, the SEM images clearly indicate that the grain size of CsPbI<sub>2</sub>Br films gradually increased from ~ 50 nm at room temperature to ~ 1 μm at 280 °C.

The as-prepared CsPbI<sub>2</sub>Br films with various annealing temperatures are also investigated by absorption spectroscopy and powder X-ray diffraction (XRD) (Figure S1). The absorption

spectra show that all the films have strong absorption from 300 nm to 650 nm wavelength range (Figure S1a). After being annealed, the absorption of films presents a peak at 640 nm.

XRD patterns (Figure S1b) show that at room temperature the film has cubic perovskite peaks at  $2\theta = 14.7, 20.9, 29.6$  and  $42.6^\circ$  which are indexed to the (100), (110), (200) and (220) planes of  $\text{CsPbI}_2\text{Br}$ , respectively. After being annealed, these diffraction peaks become stronger and sharper which confirm the improved crystallization of the perovskite films. It is important to note that when the film is annealed to  $150 - 250^\circ\text{C}$ , new peaks at  $2\theta = 12.7$  and  $38.8^\circ$  are observed. Since the new peaks are agreement with the diffraction peaks of  $\text{PbI}_2$ ,<sup>60</sup> we infer that a small amount of  $\text{CsPbI}_2\text{Br}$  subsequently decomposes. It is still unknown that what induced the decomposition, and a systematical investigation is needed in future work. However, these new peaks then disappear when annealing to  $280^\circ\text{C}$ , which indicates the decomposition products react to the cubic perovskite phase.

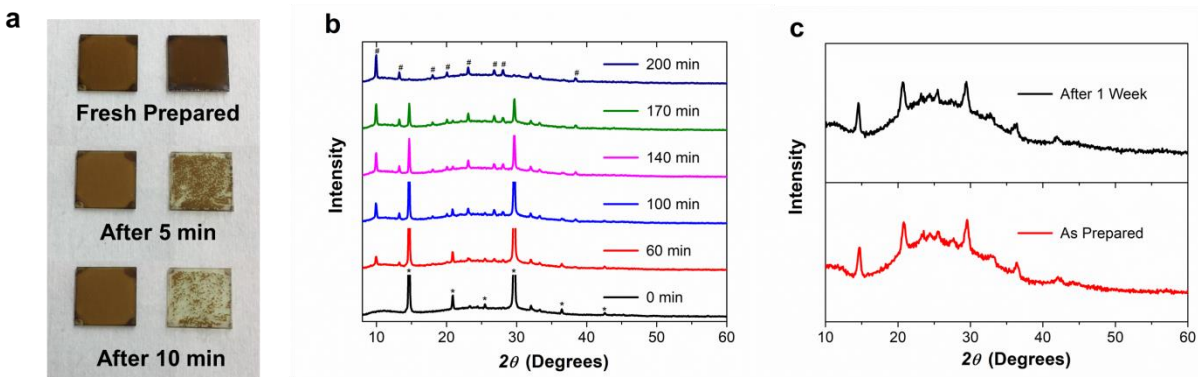


**Figure 2. Halide Perovskite Stability and Properties.** (a) Photograph of  $\text{CsPbI}_2\text{Br}$  films stored under ambient air with  $\text{RH} = 30 \pm 4\%$ . The left row is the room-temperature film; the right row is the film with  $280^\circ\text{C}$  annealing treatment. (b) XRD patterns of the film with  $280^\circ\text{C}$  annealing treatment measured continuously in ambient air with  $\text{RH} = 22 \pm 4\%$ . (c) XRD patterns of the room-temperature film before and after storage in ambient air with  $\text{RH} \leq 22 \pm 4\%$  for a week.

The humidity stability of CsPbI<sub>2</sub>Br films prepared at room temperature and 280 °C was also investigated. Figure 2a is the photograph of CsPbI<sub>2</sub>Br films before and after a short period (10 min) of storage under relative humidity (RH) of 30 ± 4% in open air, respectively. It is clear that the room temperature processed film can maintain the brown color. In contrast, the 280 °C film changes color in only 5 - 10 minutes, which suggests that the film undergoes a phase change or decomposition. The SEM image for the room temperature processed CsPbI<sub>2</sub>Br film after storage has no obvious change (Figure S2). In comparison, the 280 °C film shows a clear change with the formation of pinholes on the film surface after storage.

To further investigate the phase change of the 280 °C film under humidity, we continuously measured XRD spectra of the film under room temperature and RH = 22 ± 4% in air (Figure 2b). The initially prepared 280 °C film shows the characteristic cubic perovskite peaks. During exposure to humidity, the cubic peaks begin to fade while new diffraction peaks at  $2\theta = 10.0$ , 13.3, 26.8, 28.1 and 38.4° emerge. After 200 minutes the peaks of cubic phase completely disappear. In contrast, no change is observed in the XRD spectra for the room temperature processed CsPbI<sub>2</sub>Br film for over 1 week (Figure 2c). This indicates that the room temperature processed film has improved humidity stability and will therefore likely lead to improved operational lifetime as well.

Films with larger grain size are generally more compact than the films with small grain size, and the more compact film should have better stability because of the better resistance to the degradation from moisture and oxygen.<sup>49</sup> However, recent studies suggest that cesium lead halide perovskite films with small grain size have significantly improved stability than films with larger grain size.<sup>28-29</sup> The reduction in the number of pinholes and defect passivation on the surface are believed to be the main contributions to the improved stability. Our observation is



consistent with these studies. Previous studies also have found that grain boundaries play an important role in the perovskite film degradation process.<sup>61-62</sup> Chemical residues at the grain boundaries are suggested to be one possible reason for accelerated degradation of perovskite films. Overall, the room temperature processed technique provides an effective approach to improve the humidity stability of CsPbI<sub>2</sub>Br films.

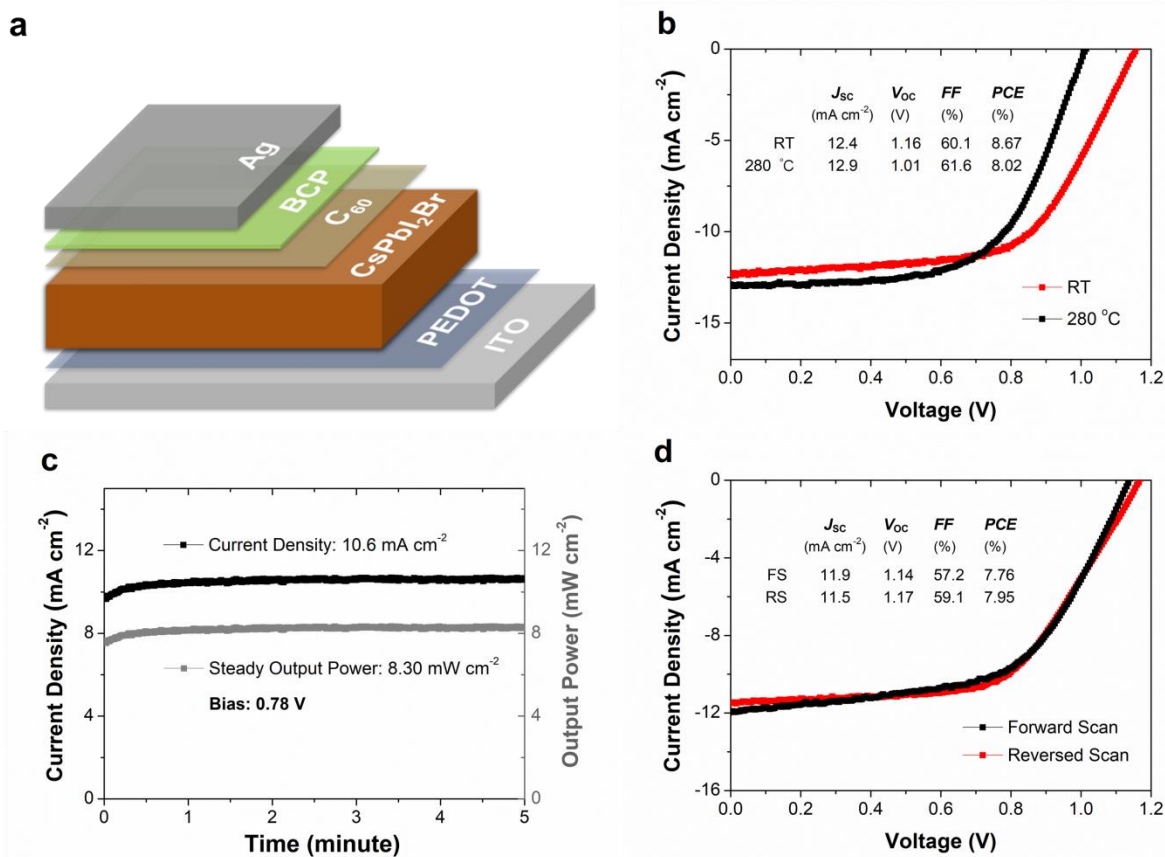


**Figure 3. Inorganic Halide Perovskite Device Performance.** (a) PSC device architecture. (b) Current–voltage ( $J$ – $V$ ) curves of perovskite devices with room-temperature CsPbI<sub>2</sub>Br film and 280 °C annealing treatment film measured under 1-sun illumination, respectively. (c) The steady current density and power output under 1-sun illumination at a bias of 0.78 V. (d) The  $J$ – $V$  curves of room-temperature processed CsPbI<sub>2</sub>Br device measured with reverse and forward bias.

Subsequently, the room temperature processed CsPbI<sub>2</sub>Br solar cells were prepared with the architecture shown in Figure 3a. A ultrathin PEDOT layer was first deposited on pre-cleaned ITO substrates. The CsPbI<sub>2</sub>Br layer was then prepared on top of the PEDOT layer by the vacuum-assist method in ambient atmosphere.<sup>48-49</sup> A 20 nm of C<sub>60</sub> and a 7.5 nm of 2,9-dimethyl-4,7-diphenyl-1,10-phenanthroline (BCP) layer were then thermally evaporated onto the CsPbI<sub>2</sub>Br layer, respectively, followed by the silver electrode.

The current–voltage ( $J$ – $V$ ) characteristics of the devices are shown in Figure 3b. Under standard AM1.5G illumination, the room temperature processed device shows a  $PCE$  of 8.67%, with a short circuit current ( $J_{SC}$ ) of 12.4 mA cm<sup>-2</sup>, a  $V_{OC}$  of 1.16 V and a fill factor ( $FF$ ) of 60.1%. The device shows an external quantum efficiency ( $EQE$ ) spectrum (Figure S3) above 60% from 390 to 620 nm. The integrated photocurrent from the  $EQE$  gives a  $J_{SC}$  of 12.1 mA cm<sup>-2</sup>, which is in good agreement with the measured value from the  $J$ – $V$  data. For the device annealed at 280 °C, a  $PCE$  of 8.02% was obtained. The lower  $PCE$  mainly stems from the loss of voltage. The  $V_{OC}$  of the 280 °C-film device is only 1.01 V which is significantly lower than the room-temperature device. The high voltage of the room-temperature device can be attributed to fewer pinholes or shunting pathways. Figure 3c shows the steady photocurrent and power output of room-temperature device is 10.6 mA cm<sup>-2</sup> and 8.30 mW cm<sup>-2</sup> under a bias of 0.78 V, respectively. Moreover, the room temperature processed device only shows a small photocurrent hysteresis when measured under forward and reversed scan mode (Figure 3d).

Based on the room temperature processing technique, inorganic cesium lead halide perovskite device were prepared on flexible substrates (Figure 4a). An ITO/poly(ethylene terephthalate) (PET) flexible substrate was used to replace the rigid ITO/glass substrate to prepare the flexible device. Figure 4b shows the  $J$ – $V$  curve of the flexible cesium lead halide perovskite solar cell.

The flexible device shows a *PCE* of 6.50% under 1-sun illumination, with a  $J_{SC}$  of 12.0 mA cm<sup>-2</sup>, a  $V_{OC}$  of 1.05 V and a *FF* of 51.4%. The unencapsulated flexible device maintained an efficiency of 6.05% after 2 months storage in inert atmosphere, which is 93% of the original efficiency.

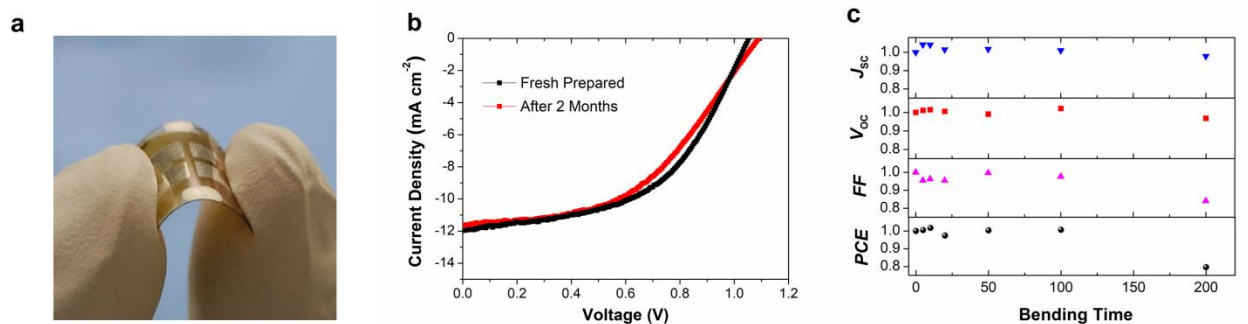


**Figure 4. All Inorganic Halide Perovskite Flexible Solar Cells.** (a)  $J$ - $V$  curves of the champion flexible CsPbI<sub>2</sub>Br device measured before and after 2 months storage in a glovebox without any encapsulation. (b) Normalized parameters of flexible CsPbI<sub>2</sub>Br devices under various bending circles with a bending radius of 4.05 mm. (c) Photograph of the flexible CsPbI<sub>2</sub>Br devices.

Bending tests were carried out to check the performance of flexible device after repeated bend cycles. After 100 bending cycles around a radius of 4.05 mm, the device only showed slight fluctuations in the efficiency (Figure 4c). However, the efficiency of the flexible device drops to ~80% after 200 bending circles, largely due to drops in the *FF* which likely stem from cracking of the ITO/PET flexible substrate. While the performance of flexible inorganic PSC can still be improved, these first demonstrations are encouraging for the development of low cost, flexible and stable inorganic perovskite solar cells.

## Conclusions

In summary, we demonstrate an approach to prepare inorganic lead perovskite films with a room temperature process. The room-temperature film shows improved humidity stability over films prepared by high temperature annealing treatment. Utilizing the room temperature approach, the inorganic lead perovskite solar cells are successfully prepared on rigid substrates and flexible substrates. This work demonstrates the integration of inorganic halide perovskites into flexible solar cells and highlights the great potential of inorganic perovskite materials for a range of flexible optoelectronic devices.

## **Experimental Section**

*Materials and Precursor Preparation:* 1-methyl-2-pyrrolidone (NMP, anhydrous, 99.5%, Aldrich.), dimethylformamide (DMF, anhydrous, 99.8%, Sigma Aldrich), dimethyl sulfoxide (DMSO, anhydrous, 99.9%, Sigma Aldrich), PEDOT:PSS (Clevios PVP AI 4083, Heraeus, diluted to 5% with water), PbI<sub>2</sub> (99%, Sigma Aldrich), CsBr (99.999%, Sigma Aldrich.), C<sub>60</sub> (99.9%, MER Corporation.) and 2,9-dimethyl-4,7-diphenyl-1,10-phenanthroline (BCP, Lumtech) were used as received.

To prepare the perovskite precursor solution, PbI<sub>2</sub>: CsBr (461 mg and 213 mg, respectively) were added in NMP (1.2 ml). The solutions were stirred for 1 hour and filtered with 0.45 μm PTFE filters before use.

*Device Fabrication:* The PEDOT layer and inorganic perovskite layer were prepared under open air conditions (with a measured relative humidity  $\leq 36 \pm 4\%$ ). The PEDOT solution was spin-coated onto pre-cleaned ITO substrates at 6000 rpm for 20 s. The perovskite precursor was spin-

coated on top of the PEDOT film at 6000 rpm for 12 s, and then moved the substrate into a homemade vacuum chamber, evacuated to  $\sim 10$  mtorr, and left in the chamber for 3 min. The samples were then transferred into glovebox. For high-temperature films, the substrates were annealed to 260-280 °C for 1 min. The substrates were then moved into the evaporation chamber for deposition of C<sub>60</sub> (20 nm) and BCP (7.5 nm). Finally, an 80 nm thick silver layer was deposited by thermal evaporation at a base pressure of  $3 \times 10^{-6}$  Torr through a shadow mask with a final measured device area of 4.85 mm<sup>2</sup>.

*Measurement and Characterization:* The current density–voltage characteristics ( $J$ – $V$  curves) were obtained using a Keithley 2420 sourcemeter under AM1.5 G solar simulation (xenon arc lamp with the spectral-mismatch factor of 0.980.) where the light intensity was measured using a NREL-calibrated Si reference cell with KG5 filter. For devices with annealing treatment, the devices were encapsulated in epoxy in glovebox before being tested due to their sensitivity to air. The room temperature films and devices, include the flexible devices, were generally tested under ambient air condition (the RH  $\leq 36 \pm 4\%$ ) without any protection or encapsulation. Devices were scanned at a rate of 50 mV s<sup>-1</sup>. The  $EQE$  measurements were performed using a QTH lamp with a monochromator, chopper, lock-in amplifier, and calibrated Si detector to measure the intensity. XRD data was measured using CuK $\alpha$  (0.154 nm) emission with a Bruker D2 phaser. The  $PL$ ,  $UV$ - $vis$  and XRD were measured on un-encapsulated samples in ambient air (the relative humidity  $\leq 22 \pm 4\%$ ). A field-emission scanning electron microscopy (Carl Zeiss Auriga Dual Column FIB SEM) was used to acquire SEM images.

AUTHOR INFORMATION

## Corresponding Author

Prof. Richard R. Lunt

\*E-mail: ([rlunt@msu.edu](mailto:rlunt@msu.edu))

Department of Chemical Engineering and Materials Science, Department of Physics and Astronomy, Michigan State University, East Lansing, Michigan 48824, USA

## ACKNOWLEDGMENT

The authors acknowledge financial support from the Michigan State University Strategic Partnership Grant (SPG) (D. L.) and from the U.S. Department of Energy (DOE) Office of Science, under Award # DE-SC0010472.

## REFERENCES

- [1] Kojima, A., Teshima, K., Shirai, Y., and Miyasaka, T. (2009). Organometal Halide Perovskites as Visible-Light Sensitizers for Photovoltaic Cells. *J Am Chem Soc* *131*, 6050-6051.
- [2] Burschka, J., Pellet, N., Moon, S.-J., Humphry-Baker, R., Gao, P., Nazeeruddin, M.K., and Gratzel, M. (2013). Sequential Deposition as A Route to High-Performance Perovskite-Sensitized Solar Cells. *Nature* *499*, 316-319.
- [3] Liu, M., Johnston, M.B., and Snaith, H.J. (2013). Efficient Planar Heterojunction Perovskite Solar Cells by Vapour Deposition. *Nature* *501*, 395-398.

[4] Zhou, H., Chen, Q., Li, G., Luo, S., Song, T.-b., Duan, H.-S., Hong, Z., You, J., Liu, Y., and Yang, Y. (2014). Interface Engineering of Highly Efficient Perovskite Solar Cells. *Science* 345, 542.

[5] Liu, D., and Kelly, T.L. (2014). Perovskite Solar Cells with A Planar Heterojunction Structure Prepared Using Room-Temperature Solution Processing Techniques. *Nat Photon* 8, 133-138.

[6] Mei, A., Li, X., Liu, L., Ku, Z., Liu, T., Rong, Y., Xu, M., Hu, M., Chen, J., Yang, Y., *et al.* (2014). A Hole-Conductor-Free, Fully Printable Mesoscopic Perovskite Solar Cell with High Stability. *Science* 345, 295.

[7] Yang, W.S., Park, B.-W., Jung, E.H., Jeon, N.J., Kim, Y.C., Lee, D.U., Shin, S.S., Seo, J., Kim, E.K., Noh, J.H., *et al.* (2017). Iodide Management in Formamidinium-Lead-Halide-Based Perovskite Layers for Efficient Solar Cells. *Science* 356, 1376-1379.

[8] (2018). <https://www.nrel.gov/pv/assets/images/efficiency-chart.png>.

[9] Eperon, G.E., Stranks, S.D., Menelaou, C., Johnston, M.B., Herz, L.M., and Snaith, H.J. (2014). Formamidinium Lead Trihalide: a Broadly Tunable Perovskite for Efficient Planar Heterojunction Solar Cells. *Energy Environ Sci* 7, 982-988.

[10] Gratzel, M. (2014). The Light and Shade of Perovskite Solar Cells. *Nat Mater* 13, 838-842.

[11] Leijtens, T., Eperon, G.E., Noel, N.K., Habisreutinger, S.N., Petrozza, A., and Snaith, H.J. (2015). Stability of Metal Halide Perovskite Solar Cells. *Adv Energy Mater* 5, 1500963.

[12] Sharma, S., Weiden, N., and Weiss, A. (1992). Phase Diagrams of Quasibinary Systems of the Type:  $ABX_3 - A' BX_3$ ;  $ABX_3 - AB' X_3$ , and  $ABX_3 - ABX' 3$ ; X = Halogen. In *Z Phys Chem*, pp. 63.

[13] Sutton, R.J., Eperon, G.E., Miranda, L., Parrott, E.S., Kamino, B.A., Patel, J.B., Hörantner, M.T., Johnston, M.B., Haghighirad, A.A., Moore, D.T., *et al.* (2016). Bandgap-Tunable Cesium Lead Halide Perovskites with High Thermal Stability for Efficient Solar Cells. *Adv Energy Mater* 6, 1502458.

[14] Beal, R.E., Slotcavage, D.J., Leijtens, T., Bowring, A.R., Belisle, R.A., Nguyen, W.H., Burkhard, G.F., Hoke, E.T., and McGehee, M.D. (2016). Cesium Lead Halide Perovskites with Improved Stability for Tandem Solar Cells. *J Phys Chem Lett* 7, 746-751.

[15] Liang, J., Wang, C., Wang, Y., Xu, Z., Lu, Z., Ma, Y., Zhu, H., Hu, Y., Xiao, C., Yi, X., *et al.* (2016). All-Inorganic Perovskite Solar Cells. *J Am Chem Soc* 138, 15829-15832.

[16] Zhang, J., Bai, D., Jin, Z., Bian, H., Wang, K., Sun, J., Wang, Q., and Liu, S. (2018). 3D–2D–0D Interface Profiling for Record Efficiency All-Inorganic CsPbBr<sub>2</sub> Perovskite Solar Cells with Superior Stability. *Adv Energy Mater*, 1703246.

[17] Zeng, Q., Zhang, X., Feng, X., Lu, S., Chen, Z., Yong, X., Redfern, S.A.T., Wei, H., Wang, H., Shen, H., *et al.* (2018). Polymer-Passivated Inorganic Cesium Lead Mixed-Halide Perovskites for Stable and Efficient Solar Cells with High Open-Circuit Voltage over 1.3 V. *Adv Mater*, 1705393.



[18] Niezgodna, J.S., Foley, B.J., Chen, A.Z., and Choi, J.J. (2017). Improved Charge Collection in Highly Efficient CsPbBr<sub>2</sub> Solar Cells with Light-Induced Dealloying. *ACS Energy Lett* 2, 1043-1049.

[19] Nam, J.K., Jung, M.S., Chai, S.U., Choi, Y.J., Kim, D., and Park, J.H. (2017). Unveiling the Crystal Formation of Cesium Lead Mixed-Halide Perovskites for Efficient and Stable Solar Cells. *J Phys Chem Lett* 8, 2936-2940.

[20] Nam, J.K., Chai, S.U., Cha, W., Choi, Y.J., Kim, W., Jung, M.S., Kwon, J., Kim, D., and Park, J.H. (2017). Potassium Incorporation for Enhanced Performance and Stability of Fully Inorganic Cesium Lead Halide Perovskite Solar Cells. *Nano Lett* 17, 2028-2033.

[21] Ma, Q., Huang, S., Chen, S., Zhang, M., Lau, C.F.J., Lockrey, M.N., Mulmudi, H.K., Shan, Y., Yao, J., Zheng, J., *et al.* (2017). The Effect of Stoichiometry on the Stability of Inorganic Cesium Lead Mixed-Halide Perovskites Solar Cells. *J Phys Chem C* 121, 19642-19649.

[22] Li, W., Rothmann, M.U., Liu, A., Wang, Z., Zhang, Y., Pascoe, A.R., Lu, J., Jiang, L., Chen, Y., Huang, F., *et al.* (2017). Phase Segregation Enhanced Ion Movement in Efficient Inorganic CsPbI<sub>2</sub> Solar Cells. *Adv Energy Mater* 7, 1700946-n/a.

[23] Frolova, L.A., Anokhin, D.V., Piryazev, A.A., Luchkin, S.Y., Dremova, N.N., Stevenson, K.J., and Troshin, P.A. (2017). Highly Efficient All-Inorganic Planar Heterojunction Perovskite Solar Cells Produced by Thermal Coevaporation of CsI and PbI<sub>2</sub>. *J Phys Chem Lett* 8, 67-72.

[24] Chen, C.-Y., Lin, H.-Y., Chiang, K.-M., Tsai, W.-L., Huang, Y.-C., Tsao, C.-S., and Lin, H.-W. (2017). All-Vacuum-Deposited Stoichiometrically Balanced Inorganic Cesium Lead

Halide Perovskite Solar Cells with Stabilized Efficiency Exceeding 11%. *Adv Mater* 29, 1605290.

[25] Swarnkar, A., Marshall, A.R., Sanhira, E.M., Chernomordik, B.D., Moore, D.T., Christians, J.A., Chakrabarti, T., and Luther, J.M. (2016). Quantum Dot–Induced Phase Stabilization of  $\alpha$ -CsPbI<sub>3</sub> Perovskite for High-Efficiency Photovoltaics. *Science* 354, 92.

[26] Wang, P., Zhang, X., Zhou, Y., Jiang, Q., Ye, Q., Chu, Z., Li, X., Yang, X., Yin, Z., and You, J. (2018). Solvent-controlled growth of inorganic perovskite films in dry environment for efficient and stable solar cells. *Nat Commun* 9, 2225.

[27] Duan, J., Zhao, Y., He, B., and Tang, Q. (2018). High - Purity Inorganic Perovskite Films for Solar Cells with 9.72 % Efficiency. *Angew Chem* 130, 3849-3853.

[28] Zhang, T., Dar, M.I., Li, G., Xu, F., Guo, N., Grätzel, M., and Zhao, Y. (2017). Bication Lead Iodide 2D Perovskite Component to Stabilize Inorganic  $\alpha$ -CsPbI<sub>3</sub> Perovskite Phase for High-Efficiency Solar Cells. *Science Advances* 3.

[29] Wang, Q., Zheng, X., Deng, Y., Zhao, J., Chen, Z., and Huang, J. (2017). Stabilizing the  $\alpha$ -Phase of CsPbI<sub>3</sub> Perovskite by Sulfobetaine Zwitterions in One-Step Spin-Coating Films. *Joule* 1, 371-382.

[30] Hu, Y., Bai, F., Liu, X., Ji, Q., Miao, X., Qiu, T., and Zhang, S. (2017). Bismuth Incorporation Stabilized  $\alpha$ -CsPbI<sub>3</sub> for Fully Inorganic Perovskite Solar Cells. *ACS Energy Lett* 2, 2219-2227.

[31] Akkerman, Q.A., Gandini, M., Di Stasio, F., Rastogi, P., Palazon, F., Bertoni, G., Ball, J.M., Prato, M., Petrozza, A., and Manna, L. (2016). Strongly Emissive Perovskite Nanocrystal Inks for High-Voltage Solar Cells. *Nat Energy* 2, 16194.

[32] Luo, P., Xia, W., Zhou, S., Sun, L., Cheng, J., Xu, C., and Lu, Y. (2016). Solvent Engineering for Ambient-Air-Processed, Phase-Stable CsPbI<sub>3</sub> in Perovskite Solar Cells. *J Phys Chem Lett* 7, 3603-3608.

[33] Eperon, G.E., Paterno, G.M., Sutton, R.J., Zampetti, A., Haghighirad, A.A., Cacialli, F., and Snaith, H.J. (2015). Inorganic Cesium Lead Iodide Perovskite Solar Cells. *J Mater Chem A* 3, 19688-19695.

[34] Wang, Y., Zhang, T., Xu, F., Li, Y., and Zhao, Y. (2017). A Facile Low Temperature Fabrication of High Performance CsPbI<sub>2</sub>Br All - Inorganic Perovskite Solar Cells. *Solar RRL* 2, 1700180.

[35] Yin, W.-J., Yan, Y., and Wei, S.-H. (2014). Anomalous Alloy Properties in Mixed Halide Perovskites. *J Phys Chem Lett* 5, 3625-3631.

[36] Docampo, P., Ball, J.M., Darwich, M., Eperon, G.E., and Snaith, H.J. (2013). Efficient Organometal Trihalide Perovskite Planar-Heterojunction Solar Cells on Flexible Polymer Substrates. *Nat Commun* 4, 2761.

[37] Roldan-Carmona, C., Malinkiewicz, O., Soriano, A., Minguez Espallargas, G., Garcia, A., Reinecke, P., Kroyer, T., Dar, M.I., Nazeeruddin, M.K., and Bolink, H.J. (2014). Flexible High Efficiency Perovskite Solar Cells. *Energy Environ Sci* 7, 994-997.

[38] Kaltenbrunner, M., Adam, G., Głowacki, E.D., Drack, M., Schwödiauer, R., Leonat, L., Apaydin, D.H., Groiss, H., Scharber, M.C., White, M.S., *et al.* (2015). Flexible High Power-Per-Weight Perovskite Solar Cells with Chromium Oxide–Metal Contacts for Improved Stability in Air. *Nat Mater* *14*, 1032.

[39] Zhang, H., Cheng, J., Lin, F., He, H., Mao, J., Wong, K.S., Jen, A.K.Y., and Choy, W.C.H. (2016). Pinhole-Free and Surface-Nanostructured NiO<sub>x</sub> Film by Room-Temperature Solution Process for High-Performance Flexible Perovskite Solar Cells with Good Stability and Reproducibility. *ACS Nano* *10*, 1503-1511.

[40] Bi, C., Chen, B., Wei, H., DeLuca, S., and Huang, J. (2017). Efficient Flexible Solar Cell based on Composition - Tailored Hybrid Perovskite. *Adv Mater* *29*, 1605900.

[41] He, Q., Yao, K., Wang, X., Xia, X., Leng, S., and Li, F. (2017). Room-Temperature and Solution-Processable Cu-Doped Nickel Oxide Nanoparticles for Efficient Hole-Transport Layers of Flexible Large-Area Perovskite Solar Cells. *ACS Appl Mater Interfaces* *9*, 41887-41897.

[42] Ling, X., Yuan, J., Liu, D., Wang, Y., Zhang, Y., Chen, S., Wu, H., Jin, F., Wu, F., Shi, G., *et al.* (2017). Room-Temperature Processed Nb<sub>2</sub>O<sub>5</sub> as the Electron-Transporting Layer for Efficient Planar Perovskite Solar Cells. *ACS Appl Mater Interfaces* *9*, 23181-23188.

[43] Wang, C., Guan, L., Zhao, D., Yu, Y., Grice, C.R., Song, Z., Awni, R.A., Chen, J., Wang, J., Zhao, X., *et al.* (2017). Water Vapor Treatment of Low-Temperature Deposited SnO<sub>2</sub> Electron Selective Layers for Efficient Flexible Perovskite Solar Cells. *ACS Energy Lett* *2*, 2118-2124.

[44] Li, K., Xiao, J., Yu, X., Li, T., Xiao, D., He, J., Zhou, P., Zhang, Y., Li, W., Ku, Z., *et al.* (2018). An Efficient, Flexible Perovskite Solar Module Exceeding 8% Prepared with An Ultrafast PbI<sub>2</sub> Deposition Rate. *Scientific Reports* 8, 442.

[45] Remeika, M., Ono, L.K., Maeda, M., Hu, Z., and Qi, Y. (2018). High-Throughput Surface Preparation for Flexible Slot Die Coated Perovskite Solar Cells. *Org Electron* 54, 72-79.

[46] Zhang, Y., Wu, Z., Li, P., Ono Luis, K., Qi, Y., Zhou, J., Shen, H., Surya, C., and Zheng, Z. (2018). Fully Solution - Processed TCO - Free Semitransparent Perovskite Solar Cells for Tandem and Flexible Applications. *Adv Energy Mater* 8, 1701569.

[47] Jeon, N.J., Noh, J.H., Kim, Y.C., Yang, W.S., Ryu, S., and Seok, S.I. (2014). Solvent Engineering for High-Performance Inorganic–Organic Hybrid Perovskite Solar Cells. *Nat Mater* 13, 897.

[48] Liu, D., Wang, Q., Traverse, C.J., Yang, C., Young, M., Kuttipillai, P.S., Lunt, S.Y., Hamann, T.W., and Lunt, R.R. (2018). Impact of Ultrathin C60 on Perovskite Photovoltaic Devices. *ACS Nano* 12, 876–883.

[49] Liu, D., Traverse, C.J., Chen, P., Elinski, M., Yang, C., Wang, L., Young, M., and Lunt, R.R. (2018). Aqueous-Containing Precursor Solutions for Efficient Perovskite Solar Cells. *Advanced Science* 5, 1700484.

[50] Chen, J., Xiong, Y., Rong, Y., Mei, A., Sheng, Y., Jiang, P., Hu, Y., Li, X., and Han, H. (2016). Solvent Effect on the Hole-Conductor-Free Fully Printable Perovskite Solar Cells. *Nano Energy* 27, 130-137.

[51] Wu, Y., Islam, A., Yang, X., Qin, C., Liu, J., Zhang, K., Peng, W., and Han, L. (2014). Retarding the Crystallization of PbI<sub>2</sub> for Highly Reproducible Planar-Structured Perovskite Solar Cells Via Sequential Deposition. *Energy Environ Sci* 7, 2934-2938.

[52] Ahn, N., Son, D.-Y., Jang, I.-H., Kang, S.M., Choi, M., and Park, N.-G. (2015). Highly Reproducible Perovskite Solar Cells with Average Efficiency of 18.3% and Best Efficiency of 19.7% Fabricated via Lewis Base Adduct of Lead(II) Iodide. *J Am Chem Soc* 137, 8696-8699.

[53] Jo, Y., Oh, K.S., Kim, M., Kim, K.-H., Lee, H., Lee, C.-W., and Kim, D.S. (2016). High Performance of Planar Perovskite Solar Cells Produced from PbI<sub>2</sub>(DMSO) and PbI<sub>2</sub>(NMP) Complexes by Intramolecular Exchange. *Adv Mater Interf* 3, 1500768-n/a.

[54] Lee, J., and Baik, S. (2018). Enhanced Crystallinity of CH<sub>3</sub>NH<sub>3</sub>PbI<sub>3</sub> by the Pre-Coordination of PbI<sub>2</sub>-DMSO Powders for Highly Reproducible and Efficient Planar Heterojunction Perovskite Solar Cells. *RSC Advances* 8, 1005-1013.

[55] Tsai, C.-M., Wu, G.-W., Narra, S., Chang, H.-M., Mohanta, N., Wu, H.-P., Wang, C.-L., and Diau, E.W.-G. (2017). Control of Preferred Orientation with Slow Crystallization for Carbon-Based Mesoscopic Perovskite Solar Cells Attaining Efficiency 15%. *J Mater Chem A* 5, 739-747.

[56] Hao, F., Stoumpos, C.C., Guo, P., Zhou, N., Marks, T.J., Chang, R.P.H., and Kanatzidis, M.G. (2015). Solvent-Mediated Crystallization of CH<sub>3</sub>NH<sub>3</sub>SnI<sub>3</sub> Films for Heterojunction Depleted Perovskite Solar Cells. *J Am Chem Soc* 137, 11445-11452.

[57] Zhou, Y., Yang, M., Wu, W., Vasiliev, A.L., Zhu, K., and Padture, N.P. (2015). Room-Temperature Crystallization of Hybrid-Perovskite Thin Films Via Solvent-Solvent Extraction for High-Performance Solar Cells. *J Mater Chem A* 3, 8178-8184.

[58] Nie, W., Tsai, H., Asadpour, R., Blancon, J.-C., Neukirch, A.J., Gupta, G., Crochet, J.J., Chhowalla, M., Tretiak, S., Alam, M.A., *et al.* (2015). High-Efficiency Solution-Processed Perovskite Solar Cells with Millimeter-Scale Grains. *Science* 347, 522.

[59] Li, X., Bi, D., Yi, C., Décoppet, J.-D., Luo, J., Zakeeruddin, S.M., Hagfeldt, A., and Grätzel, M. (2016). A Vacuum Flash-Assisted Solution Process for High-Efficiency Large-Area Perovskite Solar Cells. *Science* 353, 58-62.

[60] Liu, D., Gangishetty, M.K., and Kelly, T.L. (2014). Effect of CH<sub>3</sub>NH<sub>3</sub>PbI<sub>3</sub> Thickness on Device Efficiency in Planar Heterojunction Perovskite Solar Cells. *J Mater Chem A* 2, 19873-19881.

[61] Wang, Q., Chen, B., Liu, Y., Deng, Y., Bai, Y., Dong, Q., and Huang, J. (2017). Scaling Behavior of Moisture-Induced Grain Degradation in Polycrystalline Hybrid Perovskite Thin Films. *Energy Environ Sci* 10, 516-522.

[62] Yun, J.S., Kim, J., Young, T., Patterson, R.J., Kim, D., Seidel, J., Lim, S., Green, M.A., Huang, S., and Ho-Baillie, A. (2018). Humidity-Induced Degradation via Grain Boundaries of HC(NH<sub>2</sub>)<sub>2</sub>PbI<sub>3</sub> Planar Perovskite Solar Cells. *Adv Funct Mater*, 1705363.

## Supporting Information

# Room-Temperature Processing of Inorganic Perovskite Films to Enable Flexible Solar Cells

*Dianyi Liu<sup>1</sup>, Chenchen Yang<sup>1</sup>, Matthew Bates<sup>1</sup>, Richard R. Lunt<sup>1,2\*</sup>*

1. Department of Chemical Engineering and Materials Science, Michigan State University,

East Lansing, Michigan 48824, USA

2. Department of Physics and Astronomy, Michigan State University, East Lansing, Michigan 48824, USA



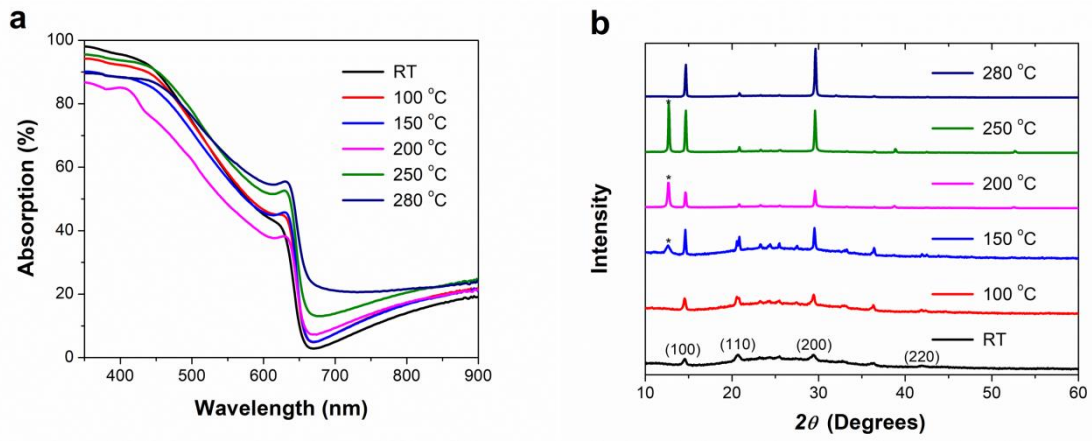


Figure S1. Absorption spectra (a) and XRD patterns (b) of CsPbI<sub>2</sub>Br films with various temperature treatments.

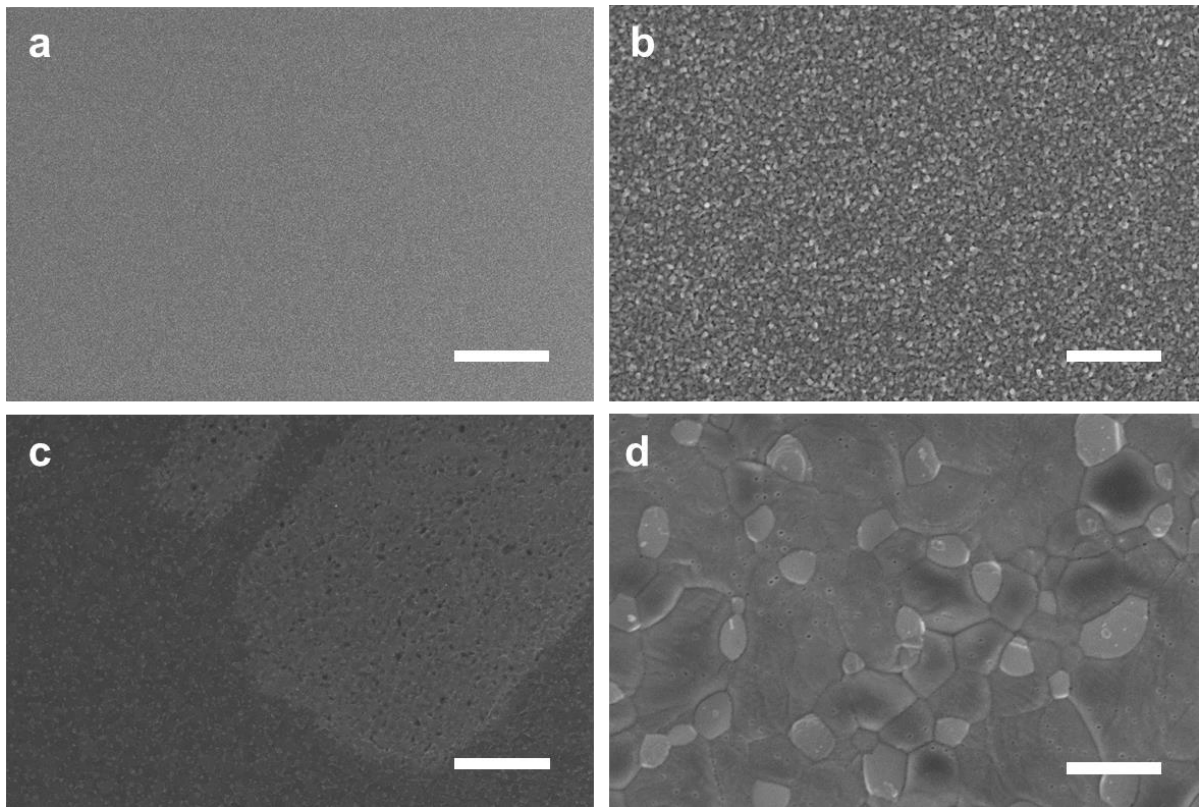


Figure S2. SEM images of CsPbI<sub>2</sub>Br film stored in ambient air (RH = 30 ± 4%) for 5 minutes. (a) and (b) is the room temperature CsPbI<sub>2</sub>Br film; (c) and (d) is the 280 °C annealing treatment CsPbI<sub>2</sub>Br film. The scale bar is 10 μm for (a) and (c), 1 μm for (b) and (d), respectively.

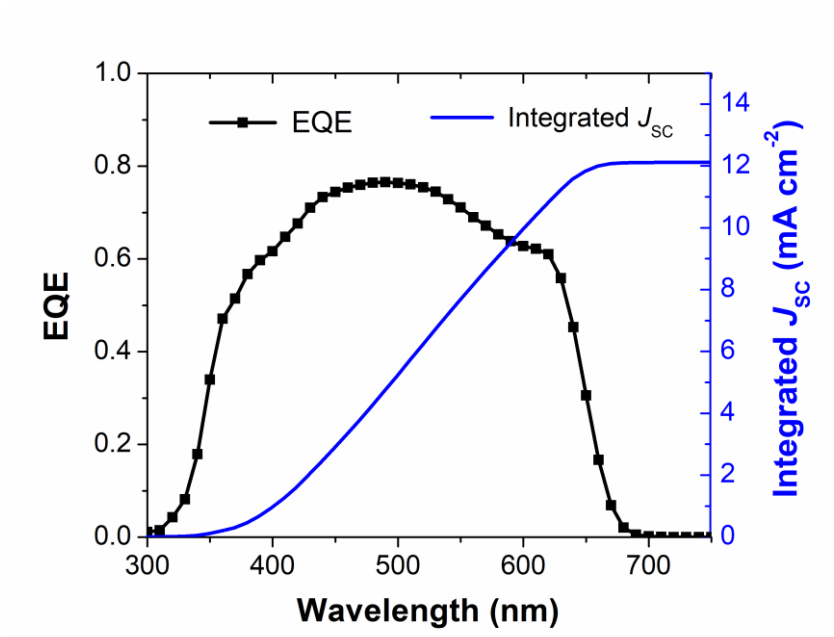


Figure S3. The *EQE* spectrum of the room-temperature CsPbI<sub>2</sub>Br devices.